Physics and Chemistry of Minerals (2024) 51:27
https://doi.org/10.1007/s00269-024-01275-8

ORIGINAL PAPER

Pressure–volume equation of state of $Fe_{18}Pt_{82}$

Meryem Berrada[1,2] · Siheng Wang[1] · Bin Chen[1] · Vitali Prakapenka[3] · Stella Chariton[3] · Marc M. Hirschmann[4] · Jie Li[2]

Received: 9 November 2023 / Accepted: 6 March 2024

Abstract
Platinum-iron (Pt-Fe) alloys have long served as oxygen fugacity sensors in high-temperature experiments investigating Earth and planetary interiors, relying on the equilibrium between Fe within the alloy and FeO in coexisting oxides or silicates. Despite their significance, studies on intermediate compositions remain limited. This investigation focuses on compressibility of $Fe_{18}Pt_{82}$ up to ~ 40 GPa at ambient temperature and explores the pressure-dependent characteristics of the oxygen fugacity relationship. In-situ X-ray diffraction measurements confirm the stability of the *fcc* phase in $Fe_{18}Pt_{82}$ across the pressure range. The fit to the compression data by the third-order Birch–Murnaghan equation of state results in $V_0 = 59.14 \pm 0.08$Å^3, $K_0 = 266 \pm 13$ GPa, and $K_0' = 4.7 \pm 0.7$. The differences between this fit and the Vinet and Kunc equations of state fall within the range of uncertainty. Comparing results with reported data for other Pt-Fe alloys reveals a nearly linear trend between volume and the Fe content in Pt-Fe alloys at ambient pressure. Unlike more iron-rich alloys, the excess volume of mixing of $Fe_{18}Pt_{82}$ (~ 0.21 cm^3/mol) remains nearly constant across the examined pressure range. Estimates of the excess Gibbs free energy suggest diminishing non-ideal contributions to thermodynamic activities as pressure increases.

Keywords Oxygen fugacity · Pt-Fe alloy · Excess volume · Gibbs free energy

Introduction

The platinum-iron (Pt-Fe) system offers a captivating platform for exploring the influence of pressure on alloy behavior—an area of research with significant implications (Kessel et al. 2001; van der Laan and Koster van Groos 1991). Among their useful properties, precious metal-iron alloys (i.e., Pt-Fe, Ir-Fe) equilibrated with Fe-bearing oxides or silicates are potentially sensitive monitors of oxygen fugacity (f_{O_2}), a key parameter in various chemical processes and of particular interest to the chemical and physical properties of deep planetary interiors (Gu et al. 2019; Gudmundsson and Wood 1995; Keefner et al. 2011; Kessel et al. 2001; Stagno et al. 2015, 2013). A fundamental reaction in the precious metal-Fe system involves Fe and O_2 interactions between alloy and silicate or oxide environments (Grove 1982; Hirschmann and Zhang 2023; Kessel et al. 2001; Taylor et al. 1992; Woodland and O'Neill 1997).

$$\underset{alloy}{Fe} + \frac{1}{2}O_2 \leftrightarrow \underset{silicate}{FeO}. \quad (1)$$

The partial pressure of oxygen in this reaction is a critical parameter that influences its equilibrium, which can be characterized by the equilibrium constant (K) and the activity coefficient of Fe in the alloys (a_{Fe}^{alloy}) and in the silicate ($a_{FeO}^{silicate}$):

$$f_{O_2} = \left(\frac{a_{FeO}^{silicate}}{K \bullet a_{Fe}^{alloy}} \right)^2. \quad (2)$$

The equilibrium may be expressed in terms of the Gibbs free energy change (ΔG):

$$K = e^{-\Delta G/RT}, \quad (3)$$

✉ Bin Chen
binchen@hawaii.edu

✉ Jie Li
jackieli@umich.edu

1 Hawai'i Institute of Geophysics and Planetology, University of Hawai'i at Manoa, Honolulu, HI, USA

2 Earth and Environmental Sciences, University of Michigan, Ann Arbor, MI, USA

3 Center for Advanced Radiation Sources, The University of Chicago, Chicago, IL, USA

4 Earth and Environmental Sciences, University of Minnesota, Minneapolis, MN, USA

Published online: 20 July 2024

where R is the gas constant, and T is temperature. Pressure (P) can influence ΔG through the volume change (ΔV) during the reaction:

$$\Delta G(P) = \Delta G\left(P_0\right) + \int_{P_0}^{P} \Delta V dP, \tag{4}$$

where P_0 is a reference pressure. The equation calculates the variation in ΔG as a function of P due to changes in V. The thermal effects remain constant across isothermal conditions, at the specific T described in Eq. 3, and are integrated within the ambient-pressure $\Delta G(P_0)$. Parameterization of ΔV requires a function with predictable behavior over a range of pressures (Michelsen and Heidemann 1996; Narayanan and Ananth 1993; Orbey and Sandler 1996). The behavior of Pt-Fe alloys may be predicted via its Equation of State (EoS). At 300 K, the third-order Birch–Murnaghan EoS (BM3) is expressed as:

$$P(V,300K) = \frac{3}{2}K_0\left[\left(\frac{V_0}{V}\right)^{\frac{7}{3}} - \left(\frac{V_0}{V}\right)^{\frac{5}{3}}\right]\left[1 + \frac{3}{4}\left(K_0' - 4\right)\left(\left(\frac{V_0}{V}\right)^{\frac{2}{3}} - 1\right)\right] \tag{5}$$

where K_0 is the isothermal bulk modulus, K_0' is the pressure derivative of the bulk modulus, V is volume, and V_0 is the zero-pressure volume (Birch 1952). Other EoS's commonly used to fit compression data at ambient temperature include the Vinet (Eq. 6) and Kunc (Eq. 7) EoS (Kunc et al. 2003; Vinet et al. 1989), the latter considers the second derivative of the bulk modulus K_0''.

$$P(V,300K) = 3K_0\left[\left(\frac{V_0}{V}\right)^{\frac{1}{3}} - 1\right]\exp\left(\frac{3}{2}\left(K_0' - 1\right)\left(1 - \left(\frac{V_0}{V}\right)^{\frac{1}{3}}\right)\right). \tag{6}$$

$$P(V,300K) = 3K_0\left[\left(\frac{V_0}{V}\right)^{\frac{1}{3}} - 1\right]\exp\left(\frac{3}{2}\left(K_0' - 1\right)\left(1 - \left(\frac{V_0}{V}\right)^{\frac{1}{3}}\right) + \frac{3}{2}K_0''\left(1 - \left(\frac{V_0}{V}\right)^{\frac{1}{3}}\right)^2\right). \tag{7}$$

These equations offer greater flexibility in capturing the complex compression behavior of materials under extreme conditions. When Fe is added to Pt and if Fe substitutes Pt atoms in the lattice (forming a substitutional alloy), the volume change might be more predictable compared to an interstitial alloy, where Fe atoms occupy interstitial spaces between Pt atoms (Matysina 1976). In general, the change in volume with increasing pressure is expected to be greater for alloys rich in Fe. This behavior is often observed in many metal alloys and is attributed to the differences in atomic size and bonding characteristics between the elements in the alloy. The substitutional scenario leads to lattice compression and a decrease in the overall volume of the alloy (Matysina 1976). When pressure is applied to the alloy, the atomic spacing is further reduced, causing an additional volume decrease. In alloys with higher Fe content, more Fe atoms are present in the lattice, and thus the overall lattice compression is more significant. Materials with a lower K_0, which describes how resistant a material is to changes in volume under the application of pressure, are more compressible and exhibit higher volume change under applied pressure. The bulk modulus of Pt-Fe alloys is thus expected to be lower for a higher Fe content. Following Vegard's Law, the excess volume of mixing (V^{xs}) is defined as the difference between the volume of the alloy and the volume expected from the individual components (Bancroft and Davis 1929; Guggenheim 1937). In the Pt-Fe alloy, this translates to:

$$V^{xs} = V_{Pt-Fe} \bullet X_{Pt-Fe} - V_{Pt} \bullet X_{Pt} - V_{Fe} \bullet X_{Fe} \tag{8}$$

where the subscripts refer to the elements, and X refers to the atomic mole fractions. The corresponding excess Gibbs free energy of mixing (G^{xs}) arises from deviations from the ideal behavior due to interactions between the components. The relationship between the partial derivative of G^{xs} with respect to pressure at constant temperature and V^{xs} follows Eq. 4 such that:

$$G^{XS} = \mathrm{G}_{\mathrm{P}_0}^{\mathrm{XS}} + \int_{P_0}^{P} V^{XS} dP, \tag{9}$$

This relationship highlights how changes in pressure can influence the excess Gibbs free energy and, consequently, the behavior of a non-ideal mixture (Michelsen and Heidemann 1996; Narayanan and Ananth 1993; Orbey and Sandler 1996). This study delves into the intricate interplay between pressure, volume changes, and alloy composition in the Pt-Fe system. By exploring how these factors impact the Gibbs free energy and alloy behavior, the discussion addresses the thermodynamic underpinnings of this system's response to pressure.

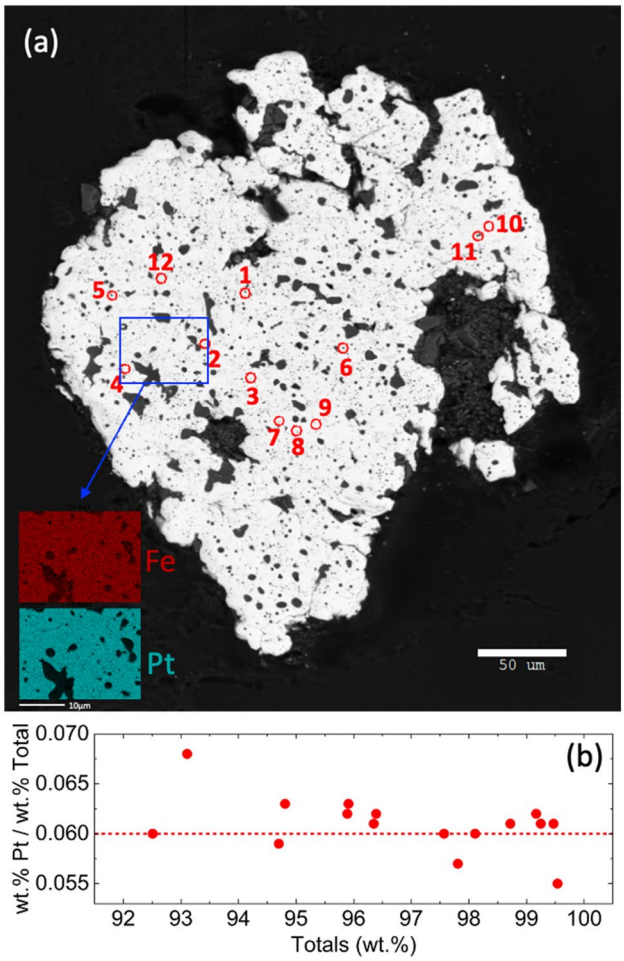

Fig. 1 **a** Backscattered image of the sample with annotated probed points. The insets show the homogeneity of the sample. **b** Ratio of wt.% Pt to Total wt.%

Methods

The starting material was synthesized by first mixing pure Fe (99.5% purity, GoodFellow Inc.) and Pt black powder (99.95% purity, Sigma Aldrich) of the desired amounts, then sintering the powder at 1673 K for 10 min to create an alloy as described in previous work (Berrada et al. 2020). A backscattered electron image of the sample is illustrated in Fig. 1. Wavelength dispersive spectrometry analysis using the Cameca SX100 Electron Microprobe instrument, with an accelerating voltage of 15 kV and focused beam of 50 nA, is reported in Table 1. Pure Pt and Fe metals were used as references for calibration. The average sample composition is found to be 94.0 ± 0.7 wt.% Pt and 6.03 ± 0.03 wt.% Fe, which corresponds to approximately Pt-18 ± 1 at.% Fe ($Fe_{18}Pt_{82}$). The sample was then loaded into a BX-90 diamond-anvil cell (DAC) equipped with 150 μm culet diamonds. The Re gasket was pre-indented to ~ 30 μm and laser drilled to create a sample chamber of 75 μm. A grain of $Fe_{18}Pt_{82}$ and a piece of gold were loaded into the sample chamber, then neon gas was loaded into the sample chamber using the gas loading system at GSECARS of the Advanced Photon Source (APS) at Argonne National Laboratory. In situ synchrotron X-ray diffraction (XRD) measurements were conducted at 300 K up to ~ 40 GPa at the 13-IDD beamline of the APS. The incident monochromatic beam had an energy of 37 keV ($\lambda = 0.335$ Å) and was focused on a spot of 3.5×2.4 μm^2. A compression membrane around the DAC provided precise *P* control. The sample *P* and corresponding uncertainties were determined using the thermal EoS of gold (Fei et al. 2007). Raw data were processed using Dioptas (Prescher and Prakapenka 2015), and PDIndexer was employed to index the integrated diffraction pattern for

Table 1 Electron microprobe analysis of the Pt-Fe sample

Point	Pt (wt.%)	Error (wt.%)	Fe (wt.%)	Error (wt.%)	Total (wt.%)
1	89.90	0.40	6.01	0.03	95.91
2	93.20	0.39	6.05	0.02	99.25
3	91.70	0.40	5.87	0.03	97.57
4	92.20	0.40	5.61	0.02	97.81
5	90.50	0.40	5.85	0.03	96.35
6	93.00	0.39	6.17	0.03	99.17
7	93.40	0.39	6.07	0.03	99.47
8	90.40	0.39	5.99	0.03	96.39
9	92.70	0.40	6.02	0.03	98.72
10	89.90	0.39	5.99	0.03	95.89
11	94.10	0.40	5.44	0.02	99.54
12	92.20	0.41	5.91	0.03	98.11
Average (wt.%)	92.1	0.6	5.91	0.03	96.83
Normalized (wt.%)	94.0	0.7	6.03	0.03	100.0
Normalized (at.%)	81.7	0.6	18.3	0.1	100.0

The error on the average is propagated with the variance formula

unit-cell parameter determination. The EoS parameters of $Fe_{18}Pt_{82}$ were derived using PythEOS (Shim 2017).

Results

The XRD peaks attributable to the Pt-Fe alloy up to ~ 40 GPa can be fitted by a structure similar to face-centered cubic (*fcc*) structure of Pt (also known as the γ phase) throughout this pressure range (Fig. 2). No evidence of ordered lower-symmetry phases (e.g., PtFe with *P4/mmm*, or Pt_3Fe with *Pm3m*), known for more Fe rich Pt-Fe alloys at low pressure was observed (Cabri et al. 2022). Figure 3a illustrates the measured unit-cell volume fit to the BM3 EoS, with corresponding uncertainty in the fitted pressure in Fig. 3b. The positive slope observed in the effective strain (f), $f = \frac{1}{2}\left[\left(\frac{V_0}{V}\right)^{\frac{2}{3}} - 1\right]$, and normalized stress (F), $F = K_0\left[1 + \frac{3}{2}\left(K_0' - 4\right)f\right]$, shown in Fig. 3c, suggests that K_0' is slightly greater than 4 up to ~ 40 GPa. Accordingly, the compressive behavior of $Fe_{18}Pt_{82}$ should be well-described by a BM3 EoS. The BM3 equation of state of $Fe_{18}Pt_{82}$ is best fit with $V_0 = 59.14 \pm 0.08 Å^3$, $K_0 = 266 \pm 13$ GPa, and $K_0' = 4.7 \pm 0.7$. As illustrated in Fig. 3d, differences between the BM3 with the Vinet and Kunc EoS suggest greater divergence from the BM3 EoS at high pressures, although within uncertainty of the BM3 EoS. The fitted parameters are summarized in Table 2. Note that the similarity in V_0 across the various EoS models is merely a coincidence.

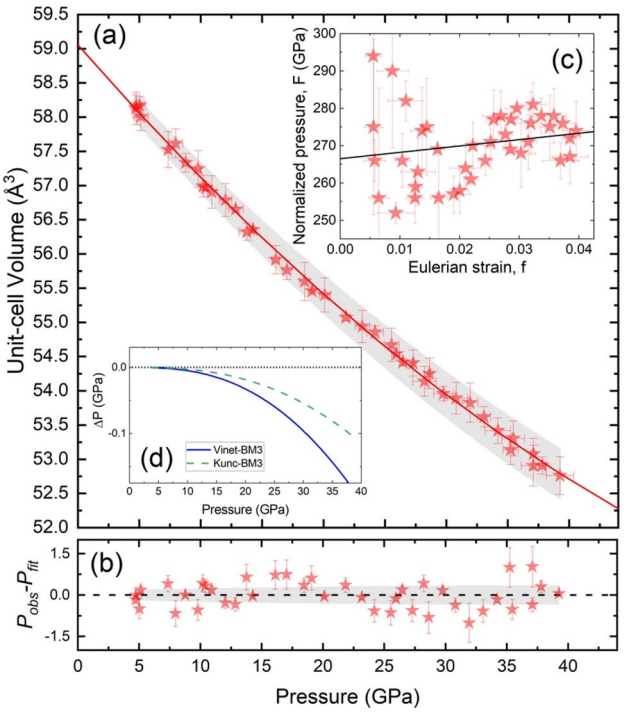

Fig. 3 **a** Unit-cell volume of $Fe_{18}Pt_{82}$ as function of pressure (filled star symbols) and the fit to the data by BM3 EoS (red curve). **b** Discrepancies between the pressure of Au (P_{obs}) and that of the sample (P_{fit}). **c** *F-f* plot with a linear fit of $F = 186(\pm 14)\text{GPa} \times f + 266(\pm 1)$ GPa. **d** Discrepancies between the EoS pressure as calculated from the Vinet and Kunc EoS models

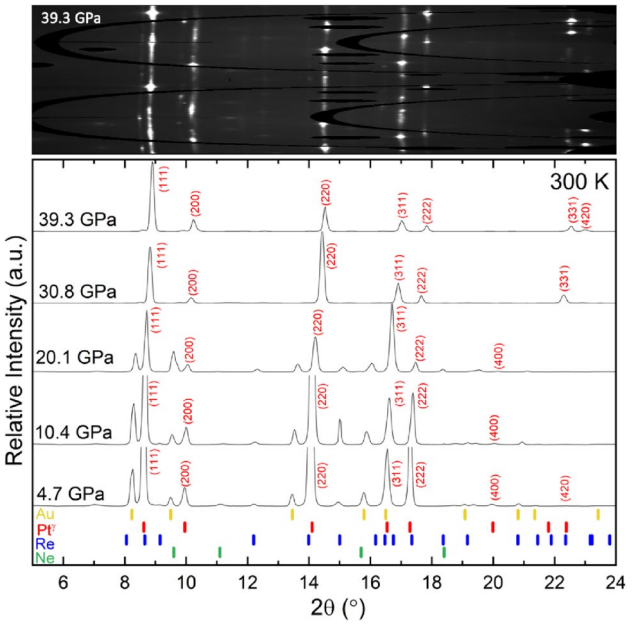

Fig. 2 Selected XRD patterns at 300K with increasing pressure, along with the cake view of 2D XRD pattern of the samples at 39.3 GPa. The sample peaks were identified from their similarities with pure Pt (γ phase)

Based on the BM3 model, the effect of Fe content on the unit-cell volume per formula of the Pt-Fe alloy is plotted in Fig. 4a, where the formula-unit volume is displayed rather than the unit-cell volume. As expected, the formula-unit volume of $Fe_{18}Pt_{82}$ is intermediate between pure Pt (Zha et al. 2008) and γ-Fe (Campbell et al. 2009; Dorogokupets et al. 2017). In combination with $Fe_{50}Pt_{50}$ (for the tetragonal structure) (Ko et al. 2009) and $Fe_{72}Pt_{28}$ (Matsushita et al. 2010), there is a near-linear relationship between the formula-unit volume and the Fe content (Fig. 4b). The linear fits of the formula-unit volumes at 100 kPa and 5 GPa are similar. Figures 4c illustrates the relation between K_0 and K_0'. While K_0 is expected to decrease with higher Fe content, the

Table 2 Equation of state parameters for the BM3, Vinet and Kunc EoS models

	BM3	Vinet	Kunc
$V_0(Å^3)$	59.14 ± 0.08	59.14 ± 0.08	59.14 ± 0.08
$K_0(GPa)$	266 ± 13	262 ± 13	263 ± 13
K_0'	4.7 ± 0.7	4.9 ± 0.7	4.8 ± 0.7

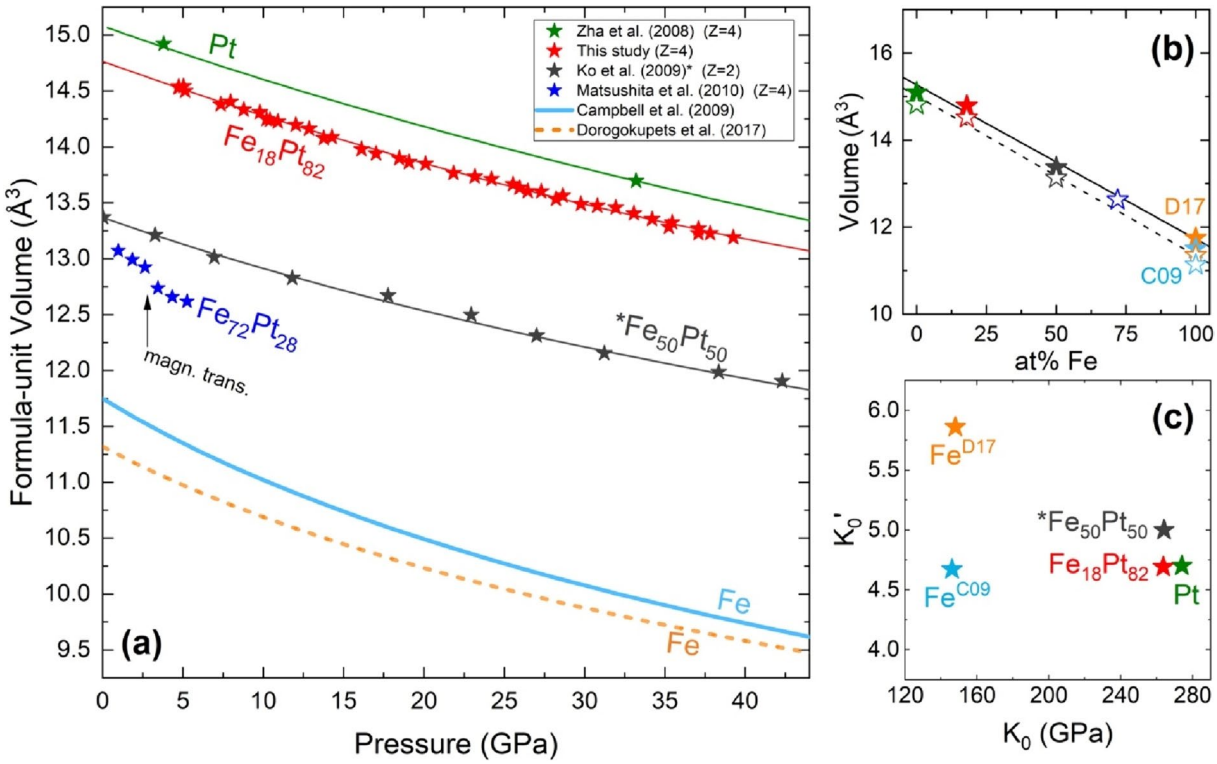

Fig. 4 **a** Survey of the EoS of Pt-Fe alloys from this study and previous work (Campbell et al. 2009; Dorogokupets et al. 2017; Ko et al. 2009; Matsushita et al. 2010; Zha et al. 2008). The Z value is displayed for references that did not report the formula-unit volumes. * Note that Ko et al. (2009) studied the ordered tetragonal phase, rather than the γ phase. "magn. trans" indicates the pressure above which this Fe-rich alloy becomes paramagnetic. **b** The formula-unit volume as a function of at.% Fe. D17 refers to Dorogokupets et al. (2017) and C09 refers to Campbell et al. (2009). The solid line shows a fit to the 100 kPa data ($V = 15.268 — 0.0354 \times X_{Fe}$). The dashed line shows a fit to the 5 GPa data ($V = 15.014 - 0.0367 \times X_{Fe}$). **c** Comparison of the bulk modulus and its first derivative of various Fe-Pt alloys. The BM3 model was used by all studies cited to obtain the EoS at 300 K

general trend is not evident. Analysis of intermediate compositions would possibly elucidate the discrepancy between the reported Fe values (Campbell et al. 2009; Dorogokupets et al. 2017).

Discussion

The EoS for $Fe_{18}Pt_{82}$ alloy determined in this study permits refinement of the thermodynamic mixing properties of Pt-Fe alloy at high pressure. To obtain V^{xs} from the EoS of $Fe_{18}Pt_{82}$, Eq. 8 is used with volumes of pure Fe from Dorogokupets et al. (2017), and pure Pt from Zha et al. (2008). At 100 kPa, V^{xs} of $Fe_{18}Pt_{82}$ is 0.36 Å^3/unit cell, or 0.21 cm^3/mol. This is slightly greater than the value of 0.18 cm^3/mol for V^{xs} of $Fe_{18}Pt_{82}$ alloy calculated from the thermodynamic mixing model of Hirschmann and Zhang (2023). Note however, that Hirschmann and Zhang (2023) calculated excess volumes relative to the EoS of Fe by Komabayashi (2014), rather than Dorogokupets et al. (2017). Calculated relative to the Fe values of Komabayashi (2014), application of Eq. 8 to the new experimentally-calibrated EoS for $Fe_{18}Pt_{82}$ would result in V^{xs} of 0.23 cm^3/mol, slightly greater than the 0.21 cm^3/mol volume calculated here. Positive values are expected for similar systems, as demonstrated in studies on Fe-Pt (Hirschmann and Zhang 2023), Fe-Pd (Matsui et al. 1983), and Fe-Ir (Woodland and O'Neill 1997) systems (Watanabe et al. 2020). On the other hand, calculating V^{xs} using a larger volume for the end members may result in a negative value. Because γ-Fe is not stable at ambient conditions, the V_0 of austenite stainless steel is sometimes used to help identify γ-Fe in powder XRD. Compared to the V_0 (298 K) of γ-Fe back-extrapolated from high-temperature measurements (Komabayashi 2014; Dorogokupets et al. 2017), austenite stainless steel ($Fe_{86.88}Cr_{13}C_{0.12}$) has a larger cell volume (V_0= 7.076 cc/mol, a = 3.609 Å^3, JCPDS card 98-000-0257; Goldschmidt 1949).

The ratio of the excess volume of mixing from that at a reference pressure of 100 kPa (V^{xs}/V_0^{xs}) remains close to unity, with no significant pressure dependence (Fig. 5a). This observation suggests that the pressure contribution to

G^{xs}, which follows Eq. 9, may be well approximated by a constant value for V^{xs}, as illustrated in Fig. 5b:

$$G^{XS} = G^{XS}_{P_0} + V^{XS}(P - P_0) \quad (10)$$

The constant value for V^{xs} is visualized in relation to the volumes of the end members and the calculated volume of $Fe_{18}Pt_{82}$, see Fig. 5c. The calculated volume $Fe_{18}Pt_{82}$ corresponds to the sum of second and third terms of Eq. 8. Equation 10 is a common approximation that has been employed to quantify the effects of pressure on non-ideal mixing of solid solutions of geological interest, including Fe alloys used as oxygen fugacity monitors (e.g., Davis and Cottrell 2021; Rubie et al. 1993; Stagno et al. 2015; Woodland and O'Neill 1997). This simplification contrasts with previous results for more Fe-rich (70–72 at.% Fe) compositions (Matsushita et al. 2004, 2010; Odin et al. 1999; Oomi and Mori 1981), for which V^{xs}/V_0^{xs} has been observed to both increase and decrease with pressure (Fig. 5a). It is unclear why present observations for the Pt-Fe alloy with 18 at.% Fe give results so distinct from the more Fe-rich compositions, or why the Fe-rich compositions produce pressure trends that are so different from one another. The Fe-rich alloys may exhibit deviations from unity in V^{xs}/V_0^{xs} beyond 5 GPa, coinciding with the Curie transition of Fe from ferromagnetic to paramagnetic at comparable pressure (Wei et al. 2017). According to Odin (1999), the volume drop in $Fe_{72}Pt_{28}$ results from high-spin to low-spin transition at 4 GPa, which precedes a magnetic collapse and thus a transition to non-magnetic state at higher pressures. The deviations from unity may also reflect alterations in electronic configurations, notably the transition from high-spin to intermediate-spin states in Fe, which manifests near 15 GPa (Zeng et al. 2008). Establishing a direct correlation between these magnetic and electronic transformations with the deviations from unity of V^{xs}/V_0^{xs} ratios presents a significant

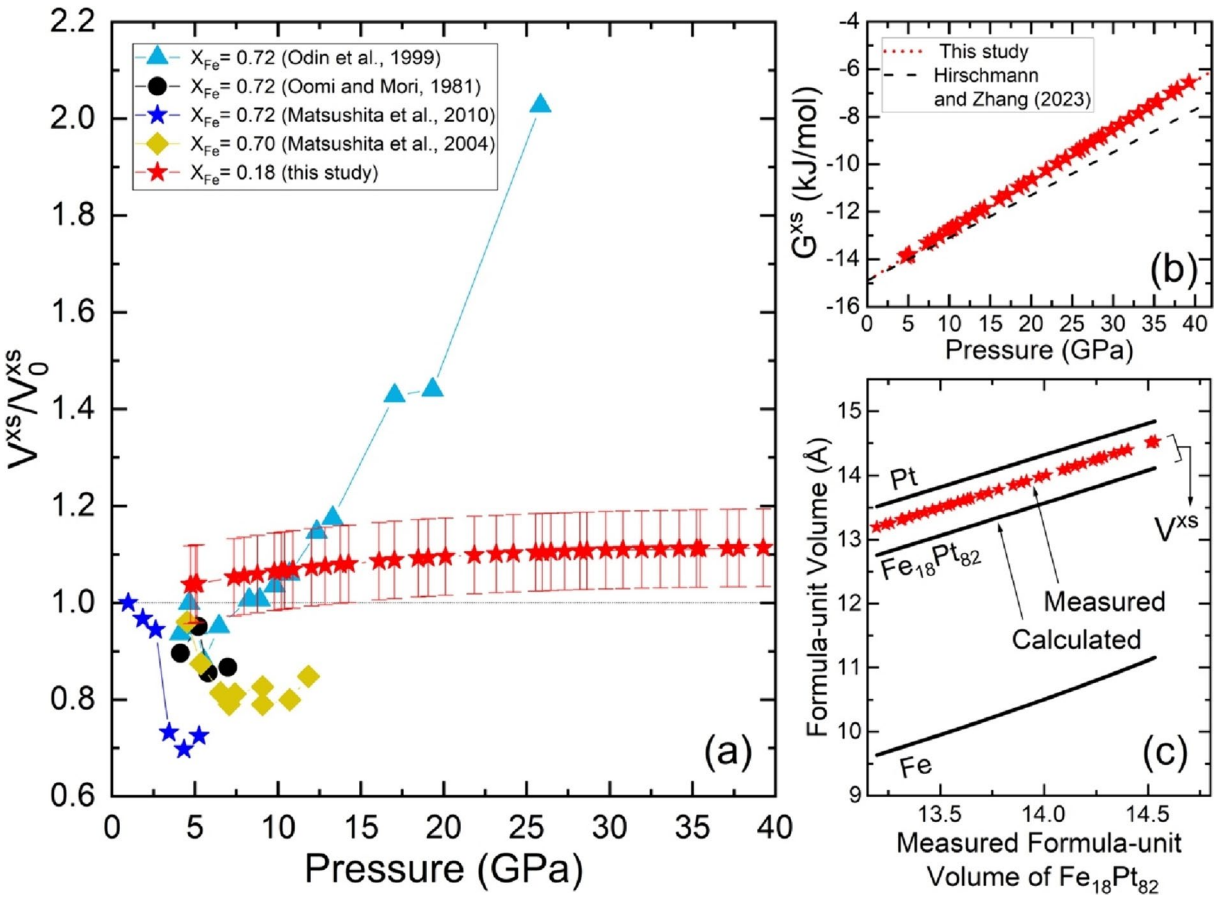

Fig. 5 **a** Calculated excess volume of mixing ratio (with a propagated uncertainty of ±0.08) as function of pressure (V^{xs}/V^{xs}_0) for this study compared with the literature (Matsushita et al. 2004, 2010; Odin et al. 1999; Oomi and Mori 1981). The unity line is displayed for reference. The propagated error on V^{xs} decreases from 0.6 at low pressures to 0.5 at high pressures. **b** The inset shows the calculated Gibbs free energy of the excess volume of mixing fit to a linear trend [$G^{XS} = P \times 0.21$ kJ/(molGPa)–14.9 kJ/mol], compared to that obtained using V^{xs} of 0.18 cm^3/mol from Hirschmann and Zhang's (2023) model [$G^{XS} = P \times 0.18$ kJ/(mol·GPa)–14.9 kJ/mol]. **c** V^{xs} is illustrated in relation with the volumes of Pt (Zha et al. 2008), Fe (Dorogokupets et al. 2017), and the calculated volume of $Fe_{18}Pt_{82}$

challenge, primarily due to the scarcity of available data at such elevated pressures. Further investigations of more Fe rich Pt-Fe alloys could clarify whether Eq. 10 remains a good approximation across the compositional binary. Nonetheless, the V^{xs} and V_0^{xs} from this study can be used to calculate G^{xs} with Eq. 10, using $G_{P_0}^{xs}$ at 100 kPa of − 14.9 kJ/mol from the Hirschmann and Zhang (2023) model at this composition. The resulting excess G^{xs} is found to increase linearly with pressure, with a slope that is modestly steeper than that predicted from the value of V^{xs} adopted by Hirschmann and Zhang (2023), see Fig. 5b. The calculated values of G^{xs} remain negative up to ~ 40 GPa, indicating sustained but diminishing negative deviations from ideality over this pressure range.

Conclusion

In light of recent advancements in the field, particularly the preliminary model proposed by Hirschmann and Zhang (2023) for characterization of f_{O_2} in high-pressure experiments, we have provided new data to improve thermodynamic characterization of Pt-Fe alloys at high pressure, but our results also highlight the need of further research to explore the EoS of Pt-Fe alloys with intermediate Fe compositions. In this study, the EoS of an intermediate composition Pt-Fe alloy, $Fe_{18}Pt_{82}$, was measured up to ~ 40 GPa at 300 K. The XRD observations confirm the stability of the *fcc* phase for this composition throughout the pressure range examined. The findings reveal a near-linear trend for V_0 of Pt-Fe alloys relative to the Fe and Pt end members. For $Fe_{18}Pt_{82}$ alloy, the calculated ratio of excess volume at pressure to that at the reference pressure,V^{xs}/V_0^{xs}, remains approximately constant and near unity up to ~ 40 GPa. This contrasts with previous results which showed both increases and decreases in V^{xs}/V_0^{xs} (Matsushita et al. 2004, 2010; Odin et al. 1999; Oomi and Mori 1981), which, if accurate, imply that complex treatments of the effect of pressure on non-ideal mixing could be required. Using the new results, calculated G^{xs} for $Fe_{18}Pt_{82}$ remains negative throughout the investigated pressure range, though its magnitude diminishes with increasing pressure. Further measurements on intermediate compositions at higher pressures and high temperatures are needed to elucidate the Fe in Pt relationship and consequently clarify pressure and temperature dependencies of f_{O_2}.

Supplementary Information The online version contains supplementary material available at https://doi.org/10.1007/s00269-024-01275-8.

Acknowledgements This work was supported by funds to M.B. from the Natural Sciences and Engineering Research Council of Canada [PDF – 567732 – 2022] and the Fonds de Recherche Nature et Technologies du Quebec [B3X 317379], and to B.C. from the National Science Foundation [EAR-1829273 and EAR-2127807] and NASA [80NSSC22K0138, 80NSSC21K0597]. J.L. and M.M.H. acknowledge support from the National Science Foundation [EAR-2317024]. This work was carried out at GeoSoilEnviroCARS (The University of Chicago, Sector 13), Advanced Photon Source, Argonne National Laboratory. GeoSoilEnviroCARS is supported by the National Science Foundation-Earth Sciences (EAR-1634415) and Department of Energy-GeoSciences (DE-FG02-94ER14466). This research used resources of the Advanced Photon Source; a U.S. Department of Energy (DOE) Office of Science User Facility operated for the DOE Office of Science by Argonne National Laboratory under Contract No. DE-AC02-06CH11357. The manuscript was improved by comments from the Editorial team and reviewers.

Author contributions Conceptualization: JL, BC; Methodology: MB, SW, BC, JL; Formal analysis and investigation: MB, MMH, SW, BC, JL; Writing – original draft preparation: MB; Writing – review and editing: MB, SW, BC, JL, MMH, VP, SC; Funding acquisition: MB, BC, JL, MMH; Resources: BC, JL; Supervision: BC, JL.

Data availability All experimental data are available at https://doi.org/10.17632/5fdjb83khv.1.

Declarations

Conflict of interest The authors declare that they have no conflict of interest.

References

Bancroft WD, Davis HL (1929) Raoult's Law. J Phys Chem 33(3):361–370. https://doi.org/10.1021/j150297a004

Berrada M, Secco RA, Yong W, Littleton JAH (2020) Electrical resistivity measurements of Fe-Si with implications for the early lunar dynamo. J Geophys Res Planets. https://doi.org/10.1029/2020JE006380

Birch F (1952) Elasticity and constitution of the Earth's interior (1896-1977). J Geophys Res 57(2):227–286. https://doi.org/10.1029/JZ057i002p00227

Cabri LJ, Oberthür T, Schumann D (2022) The mineralogy of Pt-Fe alloys and phase relations in the Pt–Fe binary system. Can Mineral 60(2):331–339. https://doi.org/10.3749/canmin.2100060

Campbell AJ, Danielson L, Righter K, Seagle CT, Wang Y, Prakapenka VB (2009) High pressure effects on the iron–iron oxide and nickel–nickel oxide oxygen fugacity buffers. Earth Planet Sci Lett 286(3):556–564. https://doi.org/10.1016/j.epsl.2009.07.022

Davis FA, Cottrell E (2021) Partitioning of Fe2O3 in peridotite partial melting experiments over a range of oxygen fugacities elucidates ferric iron systematics in mid-ocean ridge basalts and ferric iron content of the upper mantle. Contrib Miner Petrol 176(9):1–17. https://doi.org/10.1007/S00410-021-01823-3/FIGURES/11

Dorogokupets PI, Dymshits AM, Litasov KD, Sokolova TS (2017) Thermodynamics and equations of state of iron to 350 GPa and 6000 K. Sci Rep 7(1):41863. https://doi.org/10.1038/srep41863

Fei Y, Ricolleau A, Frank M, Mibe K, Shen G, Prakapenka V (2007) Toward an internally consistent pressure scale. Proc Natl Acad Sci 104(22):9182–9186. https://doi.org/10.1073/pnas.0609013104

Goldschmidt HJ (1949) Interplanar spacings of carbides in steels. Metallurgica 40:103

Grove TL (1982) Use of FePt alloys to eliminate the iron loss problem in 1 atmosphere gas mixing experiments: theoretical and practical considerations. Contrib Miner Petrol 78(3):298–304. https://doi.org/10.1007/BF00398924

Gu T, Stagno V, Fei Y (2019) Partition coefficient of phosphorus between liquid metal and silicate melt with implications for the Martian magma ocean. Phys Earth Planet Interior 295:106298. https://doi.org/10.1016/J.PEPI.2019.106298

Gudmundsson G, Wood BJ (1995) Experimental tests of garnet peridotite oxygen barometry. Contrib Miner Petrol 119(1):56–67. https://doi.org/10.1007/BF00310717

Guggenheim EA (1937) The theoretical basis of Raoult's law. Trans Faraday Soc 33:151–156. https://doi.org/10.1039/TF9373300151

Hirschmann MM, Zhang HL (2023) A revised model for activity–composition relations in solid and molten FePt alloys and a preliminary model for characterization of oxygen fugacity in high-pressure experiments. Eur J Mineral 35(5):789–803. https://doi.org/10.5194/ejm-35-789-2023

Keefner JW, Mackwell SJ, Kohlstedt DL, Heidelbach F (2011) Dependence of dislocation creep of dunite on oxygen fugacity: implications for viscosity variations in Earth's mantle. J Geophys Res Solid Earth 116(B5):5201. https://doi.org/10.1029/2010JB007748

Kessel R, Beckett JR, Stolper EM (2001) Thermodynamic properties of the Pt-Fe system. Am Mineral 86(9):1003–1014. https://doi.org/10.2138/am-2001-8-907

Ko YH, Kim KJ, Han CK, Petrovic C, Hu R, Lee HH, Lee Y (2009) Pressure–volume equation of state of FeAu and FePt. High Press Res 29(4):800–805. https://doi.org/10.1080/08957950903335513

Komabayashi T (2014) Thermodynamics of melting relations in the system Fe-FeO at high pressure: implications for oxygen in the Earth's core. J Geophys Solid Earth 119(5):4164–4177. https://doi.org/10.1002/2014JB010980

Kunc K, Loa I, Syassen K (2003) Equation of state and phonon frequency calculations of diamond at high pressures. Phys Rev B 68(9):94107. https://doi.org/10.1103/PhysRevB.68.094107

Matsui M, Shimizu T, Adachi K (1983) Invar anomalies of Fe-Pd alloys. Physica B+c 119(1–2):84–89. https://doi.org/10.1016/0378-4363(83)90171-7

Matsushita M, Nakamoto Y, Suzuki E, Miyoshi Y, Inoue H, Endo S et al (2004) The lattice softening and the crystal structure of Fe–Pt Invar alloys under high pressures. J Magn Magn Mater 284:403–408. https://doi.org/10.1016/j.jmmm.2004.07.006

Matsushita M, Inoue T, Yoshimi I, Yamaoka E, Irifune T, Ono F et al (2010) Pressure-volume-temperature relationship of Fe72Pt28 alloy under high pressure and temperature. J Phys Conf Ser 215(1):012014. https://doi.org/10.1088/1742-6596/215/1/012014

Matysina ZA (1976) Solubility in ordering alloys. Sov Phys J 19(8):1012–1020. https://doi.org/10.1007/BF00893801

Michelsen ML, Heidemann RA (1996) Some properties of equation of state mixing rules derived from excess gibbs energy expressions. Ind Eng Chem Res 35(1):278–287. https://doi.org/10.1021/ie950215v

Narayanan KV, Ananth MS (1993) Excess gibbs free energy of mixing. Fluid Phase Equilib 91(1):77–86. https://doi.org/10.1016/0378-3812(93)85080-6

Odin S, Baudelet F, Giorgetti C, Dartyge E, Itié JP, Polian A et al (1999) Magnetic phase transitions in Fe72Pt28 Invar compound studied by high-pressure X-ray magnetic circular dichroism and X-ray diffraction. Europhys Lett 47(3):378. https://doi.org/10.1209/epl/i1999-00399-6

Oomi G, Mori N (1981) Pressure effect on the spontaneous volume magnetostriction of Fe–Ni and Fe–Pt invar alloys. J Phys Soc Jpn 50(9):2924–2930. https://doi.org/10.1143/JPSJ.50.2924

Orbey H, Sandler SI (1996) Analysis of excess free energy based equations of state models. AIChE J 42(8):2327–2334. https://doi.org/10.1002/aic.690420822

Prescher C, Prakapenka VB (2015) DIOPTAS: a program for reduction of two-dimensional X-ray diffraction data and data exploration. High Press Res 35(3):223–230. https://doi.org/10.1080/08957959.2015.1059835

Rubie D, Karato S, Yan H, O'Neill HSC (1993) Low differential stress and controlled chemical environment in multianvil high-pressure experiments. Phys Chem Miner 20:315–322

Stagno V, Ojwang DO, McCammon CA, Frost DJ (2013) The oxidation state of the mantle and the extraction of carbon from Earth's interior. Nature 493(7430):84–88. https://doi.org/10.1038/nature11679

Stagno V, Frost DJ, McCammon CA, Mohseni H, Fei Y (2015) The oxygen fugacity at which graphite or diamond forms from carbonate-bearing melts in eclogitic rocks. Contrib Miner Petrol 169(2):16. https://doi.org/10.1007/s00410-015-1111-1

Taylor JR, Wall VJ, Pownceby MI (1992) The calibration and application of accurate redox sensors. Am Miner 77(3–4):284–295

Vinet P, Rose JH, Ferrante J, Smith JR (1989) Universal features of the equation of state of solids. J Phys Condens Matter 1(11):1941. https://doi.org/10.1088/0953-8984/1/11/002

Watanabe M, Adachi M, Uchikoshi M, Fukuyama H (2020) Densities of Pt–X (X: Fe Co, Ni and Cu) binary melts and thermodynamic correlations. Fluid Phase Equilib 515:112596

Wei Q, McCammon C, Gilder SA (2017) High-pressure phase transition of iron: a combined magnetic remanence and Mössbauer study. Geochem Geophys Geosyst 18:4646–4654

Woodland AB, O'Neill HSC (1997) Thermodynamic data for Fe-bearing phases obtained using noble metal alloys as redox sensors. Geochim Cosmochim Acta 61(20):4359–4366. https://doi.org/10.1016/S0016-7037(97)00247-0

Zeng Z-Y, Hu C-E, Chen X-R, Cai L-C, Jing F-Q (2008) Magnetism and phase transitions of iron under pressure. J Phys Condens Matter 20:425217

Zha C-S, Mibe K, Bassett WA, Tschauner O, Mao H-K, Hemley RJ (2008) P-V-T equation of state of platinum to 80GPa and 1900K from internal resistive heating/x-ray diffraction measurements. J Appl Phys 103(5):054908. https://doi.org/10.1063/1.2844358

van der Laan SR, Koster van Groos AF (1991) Pt-Fe alloys in experimental petrology applied to high-pressure research on Fe-bearing systems. American Mineralogist 76:1940–1949. http://pubs.geoscienceworld.org/msa/ammin/article-pdf/76/11-12/1940/4208576/am76_1940.pdf?casa_token=IkQSHrYt_jEAAAAA:BzQadutGBW2abp-0tKJVsVzkbznz6tBgMemABLWnh

Shim D (2017) Pytheos—a python tool set for equations of state. Zenodo